Conf-9006105--13

TWO-DIMENSIONAL NON-REACTING JET-GAS MIXING IN AN MHD SECOND STAGE COMBUSTOR

CONF-9006105--13

DE91 006015

S.L. Chang, S.A. Lottes and G.F. Berry
Argonne National Laboratory
9700 South Cass Avenue
Argonne, Illinois 60439

ABSTRACT

Computer simulation is used to aid in the design of a magnetohydrodynamic (MHD) second stage combustor. A two-dimensional steady state computer model, based on mass and momentum conservation laws for multiple gas species, is used to simulate the hydrodynamics of the combustor in which a jet of oxidizer is injected into a confined cross-stream gas flow. The model predicts jet-gas mixing patterns by computing the velocity and species concentration distributions in the combustor. In this paper the effects of parametric variation of jet angle and flow symmetry on the mixing patterns were evaluated. The modeling helps to determine better mixing patterns for the combustor design because improved mixing can increase combustion efficiency and enhance MHD generator performance. A parametric study reveals that (1) non-reacting jet-gas mixing strongly depends on jet angle for coflow injection (jet angle < 90 degrees), (2) counterflow jets have better jet-gas mixing, (3) asymmetry of the inlet gas flow affects the mixing pattern, and (4) exit flow characteristics from two-dimensional simulation can be matched reasonably well with experimental data when experimental jet and simulated slot jet Reynolds numbers are of the same order.

NOMENCLATURE

A	Area (m^2)
C	Mass ratio of local jet to total mixture
D	Combustor hydraulic diameter (m)
d	Jet port diameter (m)
F	Local jet concentration (or flux)
h	Slot width (m)
k	Turbulence intensity (J/kg)
L	Combustor length (m)
L_j	Jet location (m)
m_j	Jet mass flow rate (kg/s)
S	Source term in conservation equations
X	Axial coordinate (m)
Y	Vertical cross-stream coordinate (m)
Z	Horizontal cross-stream coordinate (m)
U	Velocity in X-direction (m/s)
U_0	Inlet Velocity (m/s)
V	Velocity in Y-direction (m/s)
W	Velocity in Z-direction (m/s)

Greek Letters

ε	Turbulence dissipation (J/kg-s)
Γ	Diffusion coefficient
ϕ	General flow variable
ρ	Density (kg/m^3)
σ	Normalized cross-sectional deviation
τ	Cross-sectional mean

INTRODUCTION

A magnetohydrodynamics (MHD) power plant depends upon the interaction between magnetic fields and an electrically conducting fluid flow to generate electrical power a process which can attain higher overall efficiency and produce less pollutants compared to a conventional coal-fired power plant [1-2]. Under the sponsorship of the U.S. Department of Energy, TRW is developing a 50 MWt MHD combustor [3]. The combustor is essentially a two-stage gasification device upstream of the MHD generator. The first stage consists of a pulverized coal combustion section and a deswirl section. The combustion section removes most slag and the deswirl section provides an outflow with minimal velocity profile distortion. Heat loss and NOx formation are minimized in the first stage by operating at a low equivalence ratio. The second stage combustor following the deswirl section includes oxidizer injectors and combustion chamber. Oxidizer is added in the second stage to obtain the desired plasma stoichiometry and temperature.

Among several important issues, the penetration and mixing characteristics of oxidizer jets injected into a crossflow in an MHD second stage combustor are currently under investigation. The jet-flow mixing in the second stage combustor has a large effect on the downstream generator performance. One of the major concerns is the distortion of the gas temperature profiles caused by poor mixing which may significantly lower the electric conductivity of the gas.

Recent advances in high-speed supercomputers, computational techniques to solve the coupled partial differential equations, and physical modeling, e.g., turbulence and jet mixing models [4-5], encouraged people to develop comprehensive computer models to simulate the complex jet-gas mixing in a combustor. The usefulness of such computer simulation, however, depends on the versatility, flexibility, and accuracy of the hydrodynamic models that are employed, which describe the major jet-gas mixing processes in the MHD second stage combustion chamber. While the major processes, including injection and mixing, have been the subject of on-going research, some of these processes are not well understood and comprehensive physical models are yet to be developed.

The objectives of this study are to investigate the penetration and mixing characteristics of oxidizer jets injected into a crossflow in an MHD second stage combustor with currently available two-dimensional model and to compare with the non-reacting flow experiments conducted at TRW. The model neglects the three-dimensional effects in the combustor flow field, such as asymmetric inlet flow field, inlet vortex, and jet port arrangement.

COMPUTER SIMULATION

Over the past decade, the team of Argonne National Laboratory (ANL) and University of Illinois at Chicago has developed models and associated computer codes for predicting mixing and combustion processes in air-breathing and liquid-rocket engines [6-8]. The computer code used for computation in this paper is a general two-dimensional, multi-phase, multi-species, turbulent combustion code. General conservation laws, expressed by elliptic-type partial differential equations, are used in conjunction with rate equations governing the mass, momentum, species, turbulent kinetic energy, and turbulent dissipation for the isothermal non-reacting flow case under investigation.

For convenience in numerical solution the conservation equations can be put in the form:

$$\nabla \bullet (\rho U \phi - \Gamma_\phi \nabla \phi) = S_\phi$$

The general flow variable, ϕ, is a member of the set $\{1,U,V,C,k,\varepsilon\}$. A k-$\varepsilon$ turbulence model [4] is used to model the effects of the turbulence in the flow field. A detailed description of the computer code is given in reference 8.

Flow variables are assigned values at the inlet plane and jet openings in the side walls. A reference pressure is assigned at the midpoint of the inlet plane. Patankar's [9] locally one way flow assumption is applied to the outflow boundary, eliminating the need to specify the values of flow variables at the outflow boundary. In this formulation, the streamwise diffusion coefficients are taken to be zero at the outflow boundary. The side walls are impermeable. A momentum wall function [4] is used to bridge the near wall boundary layer.

To compare different test cases with the same jet mass flow rate, the mass flow rate of the jets as well as velocity is specified from the input conditions. The jet mass flow rate is determined from the reference pressure, the specified velocity, and initial area of the jet inlet. This initial jet mass flow rate is retained in the solution by adjusting the width of the jet opening during the solution procedure to account for the difference between the reference pressure and the solved for pressure at the jet opening. The difference can be up to a few percent in the cases of this study.

A staggered and variable spaced grid system is adopted for the numerical calculation, with the gas velocity components stored on the cell surfaces and all other physical quantities stored at the nodal points of each cell (or scalar cell). The governing partial differential equations are transformed into algebraic equations by integrating over the computational cell. These algebraic equations are solved using a line-by-line sweep in the primary flow direction.

To study the effects of asymmetric inlet velocity profiles on the mixing with the jet injection, the computational grid covers a full chamber depth. A previously employed alternating direction line-by-line sweep solution method [7] was observed not to preserve symmetry in the solution when symmetric inlet profiles were employed as boundary conditions and the initial guess of flowfield variables was symmetric. Numerical experiments and analysis of the methodology revealed that line-by-line sweeps across the plane of symmetry destroyed symmetry in the intermediate results and that the asymmetry introduced became self preserving in the iterative procedure in cases of strong jet injection from the side walls.

Symmetry is achieved in the solution, however, when the line-by-line sweep is performed only in the primary flow direction. Good numerical convergence is achieved for all cases. In a typical case the normalized mass residual in a computational cell usually becomes smaller than 10^{-9} in less than 200 seconds of computing time on a CRAY-XMP supercomputer.

The mean and standard deviation of jet concentration or jet flux, used for describing the mixing development in the primary flow direction (or X-direction), are defined as follows:

Cross-Sectional Mean

$$\tau(X) = \iint F \, dA / A$$

Normalized Cross-Sectional Standard Deviation

$$\sigma(X) = [\iint (F - \tau)^2 \, dA / A]^{1/2} / \tau$$

where F can be either jet concentration or jet flux.

The standard deviation of jet concentration or flux is used as an indicator of jet-gas mixing because it is maximal where the jet and gas flows are completely separated and is zero where they are homogeneously mixed. In general, the normalized standard deviation monotonically decreases as the mixing process proceeds along the main flow direction.

Figure 1 shows the combustor under the investigation, an idealized rectangular box consisting of four solid side walls (front, back, top and bottom), a gas inlet (left), twelve jet injection holes on both top and bottom walls, and the mixture exit (right). The two-dimensional computational domain is defined in a cross-sectional area (dot line area in Fig. 1) in the middle of the combustor away from the viscous effects near the front and back walls. Two narrow openings on top and bottom walls, representing distributed injection holes, are adjustable during computation so that the total jet mass flow rate and jet velocity can be defined by input values. When the jet velocity is specified at the jet inlet, the compressibility of jet inlet conditions affects the mass conservation of jet flow because pressure is no longer a free boundary condition, but rather needs to be determined from the flow solution in the interior. A procedure added to the computer code dynamically alters the computational grid to adjust the area of the jet during iteration toward the solution in such a way that the jet mass flow rate computed matches the input value. Figure 2 shows a two-dimensional grid point system having 46 by 21 interior nodes, for which a coordinate system with an origin at the lower left corner, a horizontal X-axis, and a vertical Y-axis is defined. The evenly spaced grid points are used for the Y-axis and variably spaced grid points are defined for the X-axis depending on the jet location. Dense grid points are selected near jet opening where large flow property gradients are expected.

RESULTS AND DISCUSSION

A parametric study was conducted to investigate the effects of jet angle and inlet gas flow symmetry on the mixing pattern of the jet and the inlet gas flows. Results of the computer study indicate (1) jet-gas mixing strongly depends on jet angle in the jet angle range of 40-90 degrees, (2) counterflow jets have better jet-gas mixing and mixing is relatively insensitive to jet angle (angle > 90 degrees), and (3) asymmetry of the inlet gas flow affects the mixing pattern but has only a small effect on the extent of jet-gas mixing over the chamber length.

Effect of Jet Angle on Flow and Mixing Patterns

The jet angle is defined as the angle between the jet velocity vector and the positive X-axis. Computations with jet angles ranging from 40 to 140 degrees were performed to simulate the mixing pattern of gas and jet flows in an MHD second stage combustor. The flow conditions for these runs are based on non-reacting flow model test conditions [10] and are summarized in Table I.

Table I Simulation Conditions

Bulk Jet Concentration =	0.1556
Inlet Reynolds Number =	1.1×10^5
Jet Location (L_j/D) =	0.66
Jet velocity =	$13.7\ U_0$
Pressure =	1 atm
Temperature =	20 C
Combustor aspect ratio (L/D) =	3.84

The computed flow and mixing patterns for the two cases of 50 and 100 degree jet angle are shown in Figures 3 and 4, respectively. For each case, part "a" of the figure shows velocity vectors and part "b" shows contours of jet concentration.

For a 50 degree jet angle case, jet penetration is shallow, and consequently a region of strong convective mixing exists around the jet opening but the jet-gas mixing over the chamber width is poor. In a region from the jet opening to the exit, the jet flows are pushed toward the walls by the main stream gas flow. In this region, flow velocity is higher in the outer regions and lower in the central region, and the jets are confined in a thick layer near the walls, as shown in Figures 3a and 3b. The shear layer between the high speed jet flow and the low speed gas flow is responsible for the further mixing of the two flows by turbulent and viscous momentum transport. The shear layer is not fully developed in the combustor, evidenced by the low exit velocity in the middle as shown in Figure 3a. Experimental results show a similar velocity profile with a smaller deviation in Y-direction. The 5% jet concentration contour reaches the center line of the combustor at about X/D = 3.1 as shown in Figure 3b.

For a 130 degree jet angle case, the jet penetration is deeper and mixing is better compared with the 50 degree jet angle case. Convective jet penetration is the dominant process responsible for jet-gas mixing. Vortices are found right after the jet opening as shown in Figure 4a. The predicted vortex sizes are larger than experimental observations. The over-size predictions are believed to be caused by using the two-dimensional jet slot for the three-dimensional jet port arrangements. The 5% jet concentration contour reaches the center line of the combustor at about X/D = 1.9 as shown in

Figure 4b.

Figure 5 shows the axial development of the jet-gas mixing for three cases, 50, 100, and 130 degree jet angle. Figure 5a plots the mean jet mass concentration versus the axial (or X-axis) displacement and Figure 5b plots the normalized jet concentration standard deviation versus the axial displacement. A reference jet concentration is defined as the jet concentration of a uniform mixture of jet and gas. The reference jet concentration for these cases is 0.155.

For the 50 degree jet angle case, mean jet concentration increases along the X-axis and reaches about 0.14 at the exit as shown in Figure 5a. The exit mean jet concentration is lower than the reference jet concentration because the high jet concentration zones match the high velocity zones as shown in Fig. 3. In Figure 5b, the normalized jet concentration standard deviation for 50 degree injection decreases from about 2.6 near the injection location to about 0.6 at the exit, including a rapid convective mixing zone followed by a much slower diffusive mixing zone. The convective mixing zone is near the jet opening and mixing is primarily due to jet penetration.

For the 100 degree jet angle case, the mean jet concentration has a maximum value near X/D = 1 as shown in Figure 5a. The exit mean jet concentration is higher than 0.155, indicating lower jet concentration in higher velocity zones. The normalized jet concentration standard deviation at the exit plane is about 0.2, much lower than that of the 50 degree case. With better jet penetration, the mixing is much more complete at the end of the convective mixing zone than in the 50 degree jet angle case.

For the 130 degree jet angle case, the curves of mean jet concentration and jet concentration standard deviation are similar to those of the 100 degree case. The mean is higher than those of the 50 degree and the 100 degree cases. The deviation is much lower than that of the 50 degree case and is close to that of the 100 degree case. The jet has a large velocity component counter to the main flow direction at the injector location. The injected jet mass penetrates the upstream, is turned, and brought back downstream by interaction with the main flow. This flow configuration produces the sharp peak in mean jet concentration just upstream of the injector location shown in Figure 5a. Much of the mixing in this case occurs upstream of the injector plane. Figure 5b shows that the normalized standard deviation of jet mass concentration is about 0.7 at the injection plane for 130 degree injection, while the value for 100 degree injection is about 1.3.

For comparison, the exit velocity and jet concentration of these three cases are plotted in Figure 6. The exit velocity of 50 degree case has double humps near the walls and the exit velocities of the other two cases maximize at the center as shown in Figure 6a. The exit jet concentrations of the 100 and 130 degree cases seem more uniform than that of 50 degree case as shown in Figure 6b. The predicted exit velocity deviations are larger than experimental observations because of the over-sized vortices. Because of different exit velocity profiles, the exit mean jet concentration differs for various jet angles. The exit mean jet concentration for various jet angles are compared In Figure 7a. The exit mean jet concentration for jet angles smaller than 60 degrees is less than the reference jet concentration and for jet angles larger than 80 degrees it is greater than the reference jet concentration. In Figure 7b, the normalized standard deviation of jet flux for various jet angles is plotted. Jet-gas mixing is better for jet angles larger than 90 degrees. Jet-gas mixing depends strongly on jet injection angle for angles in the range 40 to 90 degrees, and the mixing rate increases with increasing injection angle. Above 90 degrees, the mixing rate is near optimum and only weakly dependent on injection angle.

Asymmetric Flow and Mixing Patterns

In general, the inlet gas flow velocity is asymmetric about the center line because of the non-ideal deswirl process before entering the second stage MHD combustor. Figure 8 shows the velocity vectors and jet concentration contour plots for a 130 degree case in which the inlet axial velocity changes linearly from 1.1 U_0 near Y/D = 0 to 0.9 U_0 near Y/D = 1 and other conditions remain the same as in Table I. Comparing Figures 8 and 4 reveals that for the asymmetric inlet flow case, (1) the vortex near the bottom wall, Y/D = 0, becomes larger, and (2) both maximal exit velocity and minimal exit jet concentration shift to the upper half of the chamber. In the entrance region from the inlet to approximately X/D = 1, the resultant momentum of both the inlet and the jet flows in the lower half of the chamber yields a higher pressure field compared to the upper half flows, because of the higher mass flow rate and velocity. The higher pressure field makes the main flow turn toward the upper half chamber after the jet opening. Thus, a larger vortex is formed in the lower half chamber and the velocity peak shifts to the upper half chamber.

The effect of this flow pattern on exit plane velocity and jet concentration profiles can be seen in Figure 9. For jet-gas mixing, the asymmetric case has a more uniform profile in the lower half chamber and a less uniform profile in the upper half chamber. These competing conditions yield an overall degree of jet-gas mixing which is about the same in the symmetric and asymmetric cases. The standard deviation of jet mass concentration divided by the mean is about 0.178 for the asymmetric case versus 0.167 for the symmetric case. The exit velocity profiles in Figure 9 show the shift of the peak toward the upper half chamber for the asymmetric case. This shift yields higher velocity in the upper half chamber and lower velocity in the lower half chamber. A consequence of the

velocity shift is that the standard deviation of jet mass flux, proportional to product of concentration and velocity, increases more than the standard deviation of jet mass concentration between the symmetric and asymmetric cases. The standard deviation of jet flux divided by the mean flux went from 0.211 to 0.264, an increase of 25 percent for the asymmetric case. If uniform jet flux is an important exit condition, then the degree of symmetry of the inlet gas flow becomes much more important than if only the extent of mixing of jet mass with gas is considered at the exit plane.

Comparison with experimental measurement

Experimental cold flow studies of the flow and mixing patterns in the second stage of a MHD coal-fired combustor have been conducted by TRW and are documented in References 10-12. A one-third scale transparent model of the 50 MWt combustor was used. In order to determine the degree in which the secondary oxidizer mixes with the combustion products from the first stage, injector concentration measurements were taken throughout the flow cross-section at several axial stations downstream of the injector frame.

The experimental results for a case of 130 degree jet injection with 12 injectors is shown in Figure 12. By viewing the change of the pattern of concentration contours as the flow proceeds downstream a definite rotation can be observed. This swirl cannot be modeled using the two-dimensional computer code. Therefore, data from horizontal slices in the upper plane was used because most of the rotation was observed in the lower half plane.

The inlet velocity profiles had to be estimated from knowledge of the inlet geometry, because experimental equipment configuration does not allow measurement of velocities upstream of the injector plane. At the inlet for a horizontal slice, the turning flow from the deswirl section of the first stage combustor is expected to have a positive component of velocity in the Z-direction (toward the outer wall of the turn) and a lower X velocity. For the X-direction (U) velocity, simulations were done with the maximum at various percentages above the mean. A value of ten percent produces a good match to the experimental result at Y/D = 0.667, and the results are not very sensitive to U_{max}/U_{mean} in the range (1.01 to 1.2). Similar comments apply to the Z-component of velocity (W). This component was given a flat profile in the mid half section of the chamber decreasing linearly to zero in the quarter of the range near the walls. A value of W_{max}/U_{mean} of 0.1 appears to produce best correspondence with the experimental result at (Y/D = 0.667), but again the results are not very sensitive to the value of W_{max}/U_{mean} in the range 0.01 to 0.2.

The greatest problem in matching the results was to simulate the correct jet penetration depth. If the simulated jet total injection flow rate matches the total injection flow rate, the simulated jet mass flow rate equals the measured jet mass flow rate and the simulated jet velocities equal the measured jet velocities, then the simulated jet penetration depth is much too shallow. This shortfall is attributed to the fact that distributing the round jets as a simulated slot increases the jet perimeter by a factor of 2.8 and decreases the jet width by a factor of 0.04. These two factors allow cross-stream momentum from the main flow to penetrate the simulated jet slot much too quickly.

Table II Relationship Between Jet Flow Rate, Slot Width and Reynolds Number

	m_j (kg/s)	h/d	Re_{jr}/Re_{js}
a	0.01	0.04	5.2
b	0.03	0.12	1.7
c	0.06	0.24	.86

To overcome this difficulty both the jet velocity and jet slot width were varied. Due to numerical difficulties caused by backflow, the highest jet velocity that could be used was approximately 600 m/s. Using three different jet widths indicated in Table II, the results shown in Figure 12 were obtained. The jet flow rate of 0.01 kg/s corresponds to the experimental jet flow value. For a flow rate of 0.06 kg/s, the results compare reasonably well with experimental data. This is clearly shown in Figure 14. Table III shows the ratio of the round jet Reynolds number, Re_{jr}, to the Reynolds number of the slot, Re_{js}, for the three simulations plotted in Figure 14. Simulation with a slot Re_{js} close to experimental Re_{jr} produces comparable jet penetration and exit velocity profile.

Numerical Convergence

In a typical computation, the mass residual of each cell in the computational domain is checked after each iteration of solving mass, momentum and energy equations. The mass residual is required to be smaller than a preset convergence criterion before stopping the iteration. If the process converges, mass residual becomes smaller as the iteration goes on. Figure 11 shows the convergence behavior of a typical computation. Note that normalized mass residual is defined as the ratio of mass residual to the exit mass flow rate. The maximum mass residual decreases from 10^{-5} in 50 iterations to 10^{-15} in 1400 iterations. After 1400 iterations, the convergence can not be further improved due to the floating point precision of the CRAY supercomputer. Each iteration takes approximately 0.25 second of computing time and a typical convergent case needs about 200 seconds of supercomputing time to reduce the maximum normalized mass residual to less than 10^{-9}.

CONCLUSION

A computer simulation program using comprehensive physical models to investigate the penetration and mixing characteristics of oxidizer jets injected into a crossflow in an MHD second stage combustor has been developed on ANL's CRAY X-MP supercomputer. The model computes the velocity and species concentration distributions in the combustor and predicts non-reacting jet-gas mixing patterns. The modeling helps us understand the mixing patterns for the combustor and allows us to suggest design which can improve combustion efficiency and enhance MHD generator performance. A parametric study using the computer code was conducted to evaluate the effects of jet angle and inlet gas flow asymmetry on the mixing pattern of the jet and the inlet gas flows. The findings include (1) jet-gas mixing strongly depends on jet angle for coflow injection (jet angle < 90 degrees), (2) counterflow jets have better jet-gas mixing and mixing is relatively insensitive to jet angle (angle > 90 degrees), (3) asymmetry of the inlet gas flow affects the mixing pattern but has only a small effect on the level of jet mass mixing over the chamber length, and (4) exit flow characteristics from two-dimensional simulation can be matched reasonably well with experimental data when experimental jet and simulated slot jet Reynolds numbers are of the same order.

ACKNOWLEDGEMENT

This work was supported by U.S. Department of Energy, Assistant Secretary for Fossil Energy, Under Contract W-31-109-ENG-38. The authors thank Mr. Andrew Grove of TRW for his valuable comments and Mr. Paul Lissac for his assistance in preparing the figures.

REFERENCES

[1] Chang, S.L., G.F. Berry, and N. Hu, "System Analysis of High Performance MHD Systems," Prec. of 23rd Intersociety Energy Conversion Engineering Conference, Vol. 4, pp. 455-459 (1988).

[2] Carter C. and J.B. Heywood, "Optimization Studies on Open-Cycle MHD Generators," AIAA Journal, Vol. 6, pp. 1703-1711 (1968).

[3] "Coal-Fired MHD Combustor Development Project: Phase IIIB", DOE Report DE87003845 (1987).

[4] Launder, B.E., and D.B. Spalding, "The Numerical Computation of Turbulent Flows," Computer Methods in Applied Mechanics and Engineering, Vol. 3, pp. 269-289 (1974).

[5] Patankar, S.V., D.K. Basu, and S.A. Alpay, "Prediction of the Three-Dimensional Velocity Field of a Deflected Turbulent Jet," Journal of Fluids Engineering, 99:758-762 (1977).

[6] Zhou, X.Q., and H. Chiu, "Spray Group Combustion Processes in Air Breathing Propulsion Combustors," Paper AIAA-83-1323, AIAA/SAE/ASME 19th Joint Propulsion Conference, Seattle, Washington (1983).

[7] Lottes, S.A., "Unsteady Group Combustion," Ph.D. Thesis, University of Illinois at Chicago, Chicago, Illinois (1989).

[8] Jiang, T.L., and H.H. Chiu, "Advanced Modeling of Spray Combustion Process in Air Breathing Propulsion Combustors," AIAA-87-0067, AIAA 25th Aerospace Science Meeting, Reno, Nevada (1987).

[9] Patankar, S.V., "Numerical Heat Transfer and Fluid Flow," McGraw-Hill Book Company (1980).

[10] Grove, A., et. al., "Cold Flow Modeling Study of Coal-Fired MHD Combustor," 26th Symposium on Engineering Aspects of Magnetohydrodynamics, Nashville, AL (1988).

[11] Grove, A., "Cold Flow Mixing Study of 50 MWt MHD Coal-Fired Combustor Second Stage," 27th Symposium on Engineering Aspects of Magnetohydrodynamics, Reno, NV (1989).

[12] Grove, A., et. al., "Cold Flow Mixing Study of an MHD Combustor Model Using Laser Velocimeter and Concentration Measurements," 28th Symposium on Engineering Aspects of Magnetohydrodynamics, Chicago, IL (1990).

DISCLAIMER

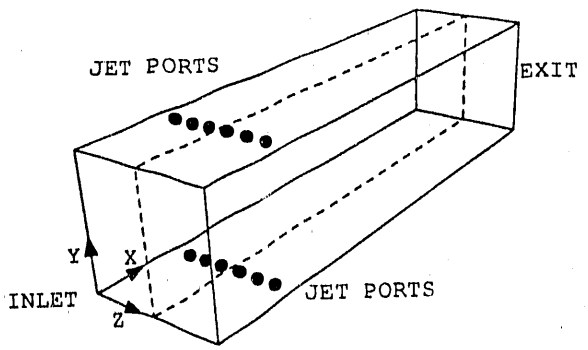

Figure 1 Idealized combustor geometry, MHD second stage, (12-jet)

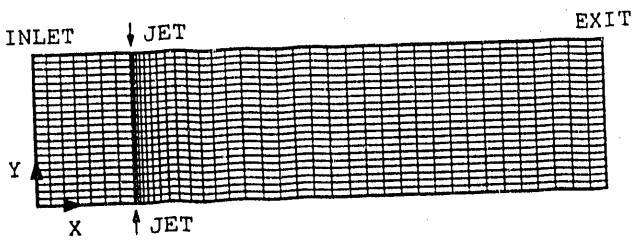

Figure 2 Two-dimensional grid system (46 by 21 nodes)

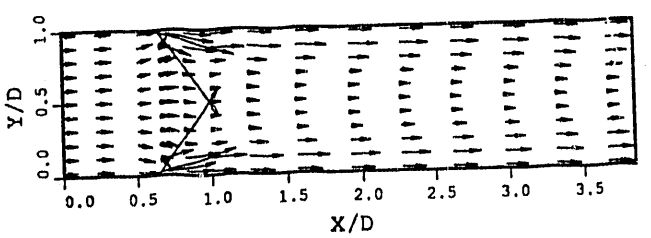

(a) Velocity vectors

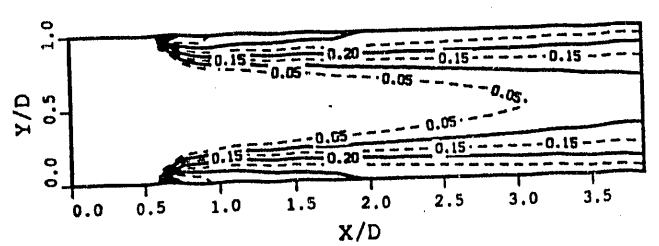

(b) Jet concentration contours

Figure 3 Flow and mixing patterns (50 Degree jet angle)

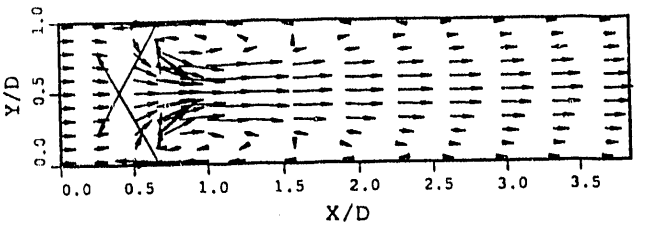

(a) Velocity vectors

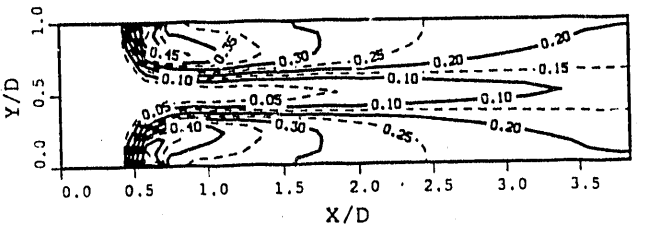

(b) Jet concentration contours

Figure 4 Flow and mixing patterns (130 Degree jet angle)

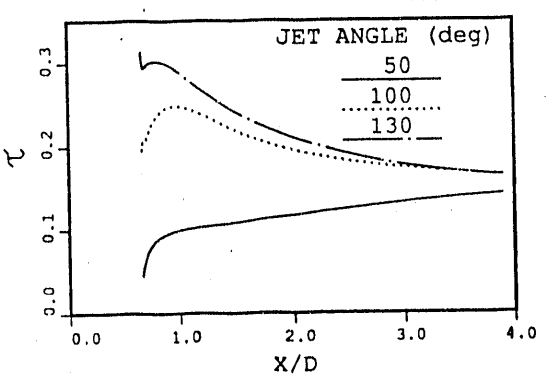

(a) Mean jet concentration

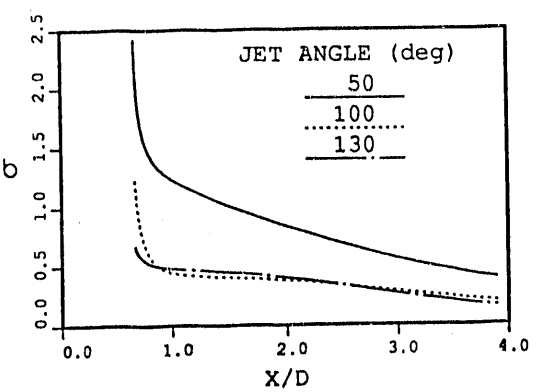

(b) Deviation of jet concentration

Figure 5 Axial development of symmetric jet-gas mixing for various jet angles

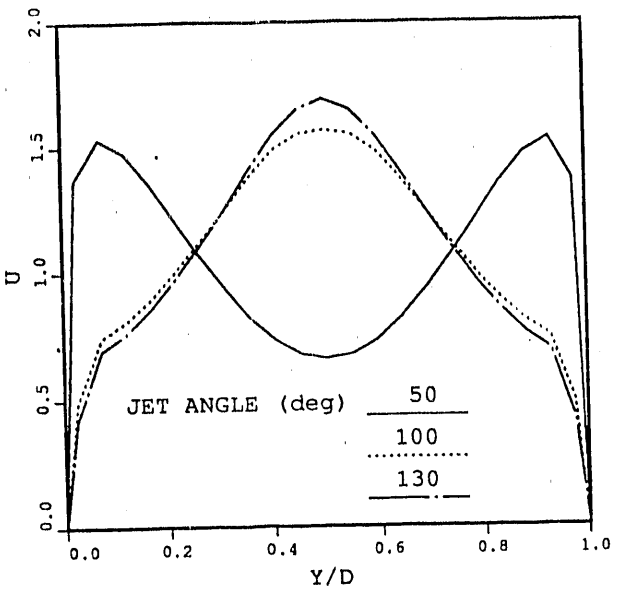

(a) Exit axial velocity

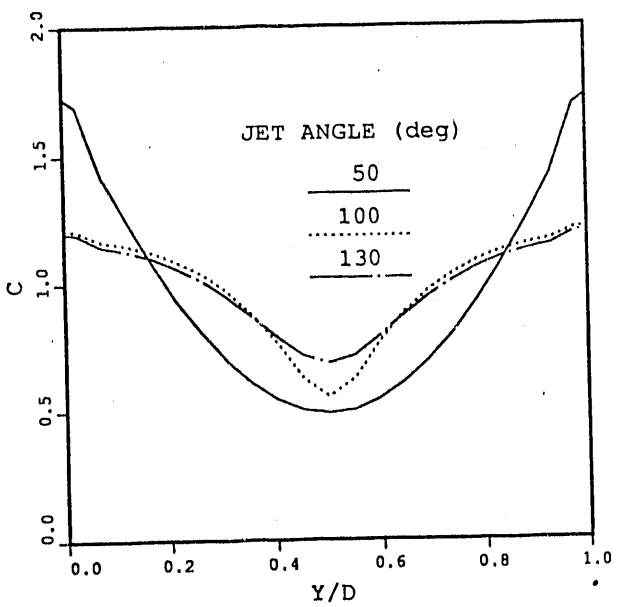

(b) Exit jet concentration

Figure 6 Normalized exit flow and mixing profiles for various jet angles

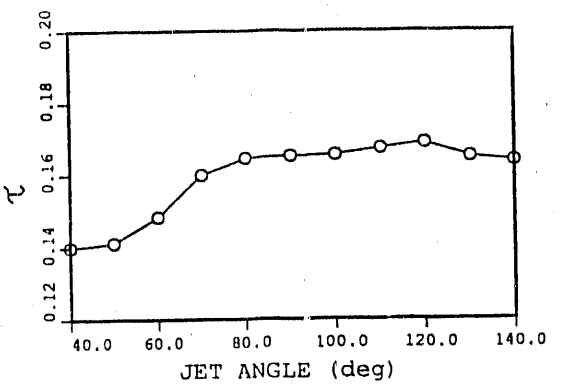

(a) Mean jet concentration

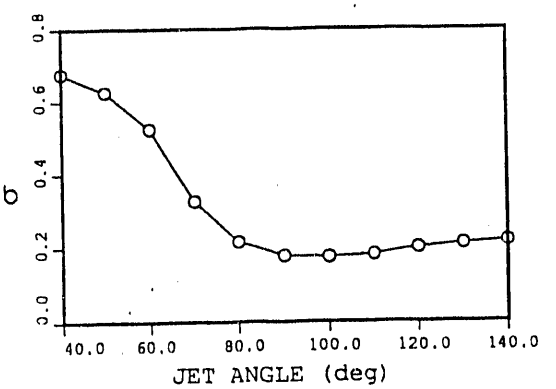

(b) Deviation of jet concentration

Figure 7 Effect of jet angle on jet-gas mixing at the exit

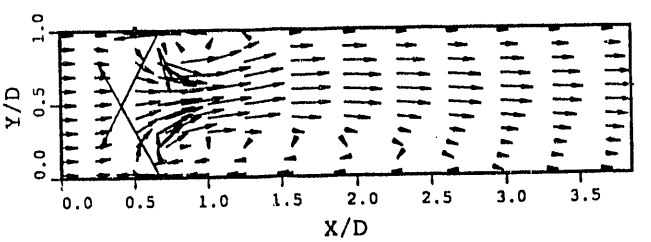

(a) Velocity vectors

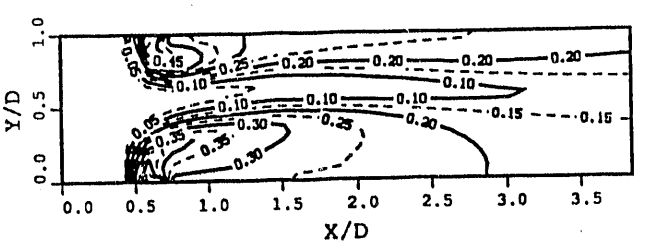

(b) Jet concentration contours

Figure 8 Asymmetric flow and mixing patterns

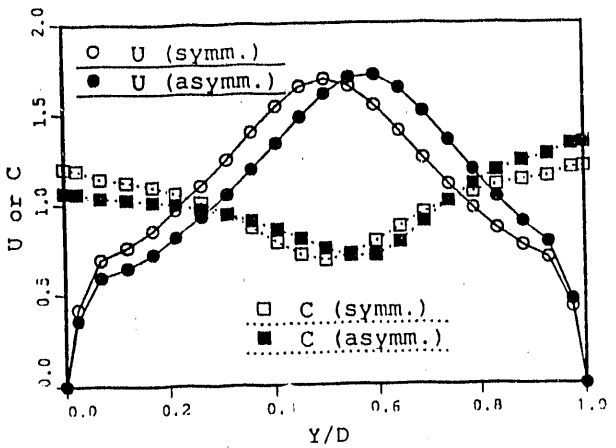

Figure 9 Exit flow and cocentration profiles for symmetric and asymmetric flows

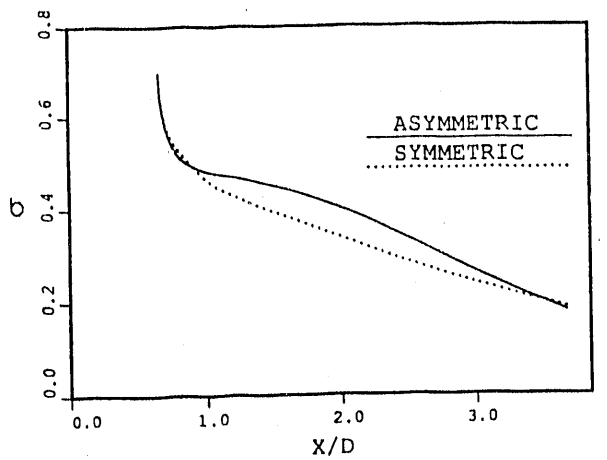

Figure 10 Asymmetric effect on axial development of jet-gas mixing

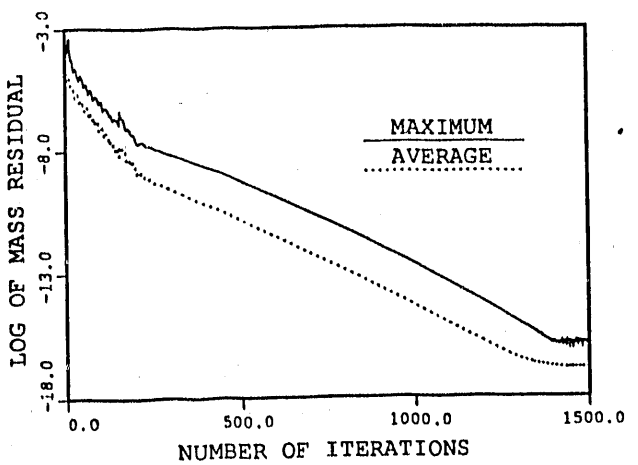

Fgiure 11 Numerical convergence

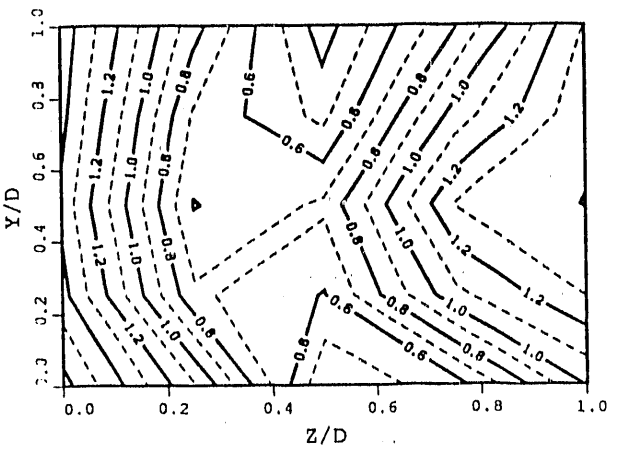

(a) X/D = 1.8

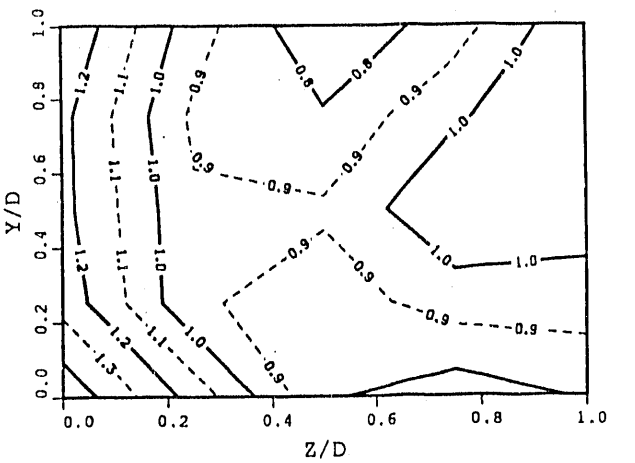

(b) X/D = 2.8

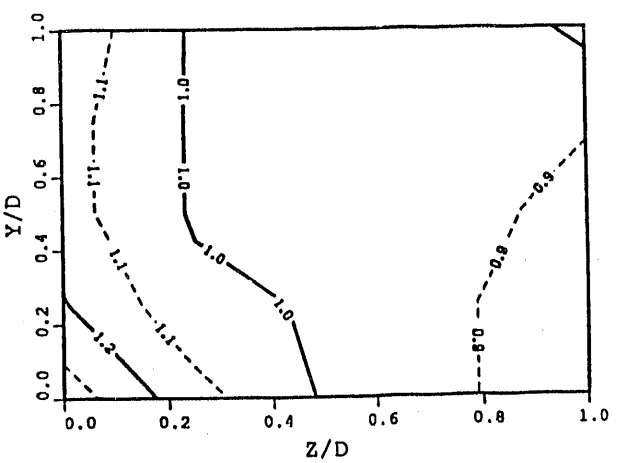

(c) X/D = 3.8

Figure 12 TRW oxygen DATA contours

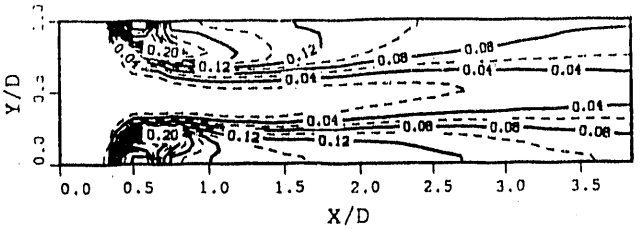

(a) Jet flow rate = 0.01 kg/s

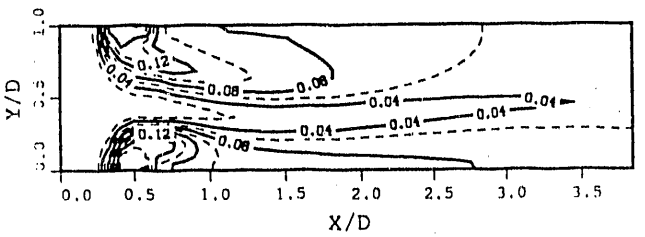

(b) Jet flow rate = 0.03 kg/s

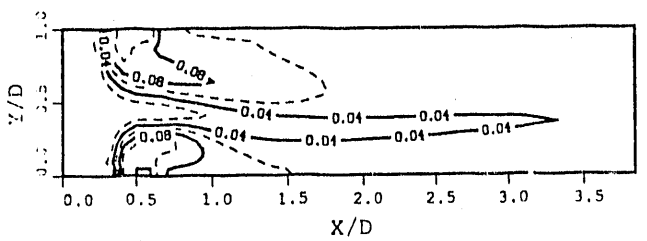

(c) Jet flow rate = 0.06 kg/s

Figure 13 Asymmetric mixing patterns

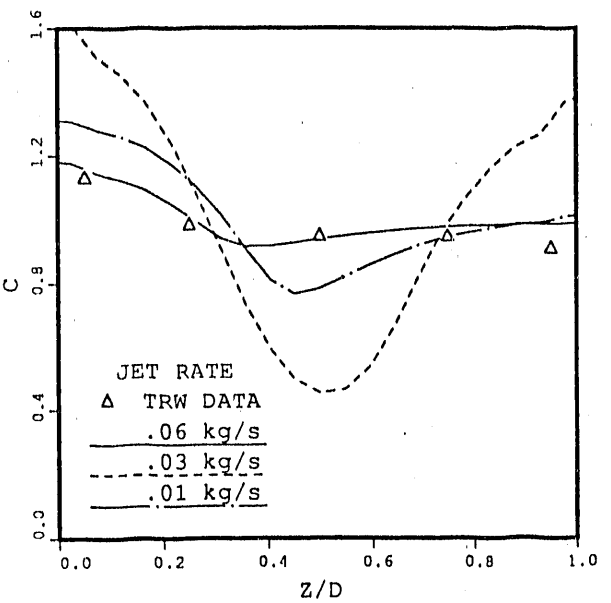

Figure 14 Comparison of exit jet concentration profiles

-END-

DATE FILMED

02/20/91